Int J Thermophys (2010) 31:1935–1944
DOI 10.1007/s10765-008-0523-9

Thermal Conductivity and Interfacial Thermal Resistance in Bilayered Nanofilms by Nonequilibrium Molecular Dynamics Simulations

Shuaichuang Wang · Xingang Liang

Published online: 1 November 2008
© Springer Science+Business Media, LLC 2008

Abstract A nonequilibrium molecular dynamics study of the cross-plane thermal conductivity and interfacial thermal resistance of nanoscale bilayered films is presented. The films under study are composed of argon and another material that is identical to argon except for its atomic mass. The results show that a large temperature jump occurs at the interface and that the interfacial thermal resistance plays an important role in heat conduction for the whole films. The cross-plane thermal conductivity is dependent on the average temperature. The interfacial thermal resistance is found to be dependent apparently on the atomic mass ratio of the two materials and the temperature, but to be independent of the film thickness. A linear relationship is observed between the reciprocal of the cross-plane thermal conductivity and that of the film thickness with the film thickness between 5.4 nm and 64.9 nm, which is in good agreement with results in the literature for a single film.

Keywords Interface · Molecular dynamics · Thermal conductivity · Thermal resistance

1 Introduction

Of late, the rapid progress in synthesis and fabrication technology has made the scientific understanding of thermal transport in nanoscale multilayered films to be of fundamental significance and of practical importance. Interfaces between thin films play a crucial role in determining the performances of many structures and devices at

S. Wang · X. Liang (✉)
Department of Engineering Mechanics, Key Laboratory for Thermal Science and Power Engineering, Ministry of Education of China, Tsinghua University, Beijing 100084, China
e-mail: liangxg@tsinghua.edu.cn

the microscale. Generally, the transfer of thermal energy in a solid is accomplished by heat carriers, e.g., phonons for dielectric materials. When a heat carrier encounters an interface, it must take more effort to get across the interface. It means that there is a thermal resistance at the interface. In the presence of a heat current, a temperature discontinuity will occur at the interface between two different materials or at the grain boundary. As early as 1941, Kapitza [1] noticed this phenomenon and measured the temperature drop at the interface between copper and liquid helium. The interfacial thermal resistance is known as the Kapitza resistance, which is defined as

$$R_{\kappa} = \Delta T / J, \tag{1}$$

where ΔT is the temperature difference across the interface and J is the heat flux across the interface. The inverse of the Kapitza resistance is called the Kapitza conductance.

There are two theoretical models to describe the interfacial thermal resistance between two solids, the acoustic mismatch model (AMM) [2] and the diffuse mismatch model (DMM) [3]. The former is derived from continuum acoustics, and assumes that phonons propagate as a plane wave. The energy transmission probability is related with the acoustic impedances of the materials on the two sides. The latter is on the complementary extreme and assumes that all phonons colliding into the interface are randomly scattered. The transmission probability of the phonons is proportional to the phonon density of states of the two materials. For most interfaces between two materials, the AMM and DMM show good agreement with low-temperature experiments [3], but are in poor agreement with experimental results for comparatively high temperatures [4].

There are several experimental studies of the interfacial thermal resistance between dissimilar solids [5–7]. The values of the interfacial conductance determined by Costescu et al. [6] are in good agreement with the predictions of the DMM. But the values obtained by Stoner and Maris [5] are four times larger than those by Lyeo and Cahill [7] at the same condition. Experimental results generally are affected by some uncertain factors, and it is hard to control the structure of the interface.

From the above discussion, it could be concluded that the mechanism and prediction of the interface resistance between two dissimilar materials are not well understood theoretically. The molecular dynamics (MD) technique is another choice of research methods because creating a suitable interface and measuring the thermal properties of a composite film can be achieved easily in MD simulation. The MD simulation by Maiti et al. [8] showed a significant interfacial resistance at a symmetric tilt grain boundary. Schelling et al. [9] found that the Kapitza resistance of a twist grain boundary increases with increasing grain boundary energy. The interfacial resistance effects on the thermal conductivity were also mentioned to explain the mechanism of the thermal conductivity in the superlattice [10,11] and heterostructure [12]. Chen et al. [13] simulated the lattice thermal conductivities of Ar and Ar/Kr nanostructures. Their results show that the interface scattering poses a significant resistance to the phonon transport in the superlattices and superlattice nanowires. They explicitly calculated the interfacial thermal resistance and found that it increases with the period length for a given total length of 48 unit cells. The authors attributed this increase to the interface strain due to the mismatch of lattice constants. Liang and Sun [14] showed that the

interface roughness has significant impact on the interfacial thermal resistance. This study employs nonequilibrium molecular dynamics method (NEMD) to investigate the effective cross-plane thermal conductivity and interfacial thermal resistance between two Ar-type dissimilar materials.

2 MD Simulation Model

A three-dimensional composite film is constructed to study the interfacial properties using two dielectric thin layers, layer A and layer B, along the x direction. Figure 1 shows the configuration sketch. Layer A is solid argon, which has the structure of the fcc lattice, and layer B is the same as layer A except for its atomic mass. Without special description, the atomic mass of layer B is four times heavier than that of layer A. The interface between the two materials is in the (100) plane, that is, the cross plane is the <100> direction. All atoms interact with each other through the classical Lennard-Jones (12-6) potential [15]:

$$\phi(r) = 4\varepsilon\left[\left(\frac{\sigma}{r}\right)^{12} - \left(\frac{\sigma}{r}\right)^{6}\right] \tag{2}$$

where r is the distance between the pair of atoms to be considered, the parameter $\varepsilon = 1.67 \times 10^{-21}$ J is the well depth, and the parameter $\sigma = 3.4 \times 10^{-10}$ m is the equilibrium separation.

The bilayered film is confined between solid walls, both of which are one unit cell (UC) in thickness to prevent any atom from escaping from the simulation system. A heat source and a sink are imposed close to the solid walls at the two ends in the x direction, and both thicknesses are two UC. The temperatures of the heat source and sink are fixed at T_1 and T_2 using the velocity-scaling method with the conservation of momentum [16]. It is convenient to calculate the energy $\Delta\varepsilon_1$ added to the source and the energy $\Delta\varepsilon_2$ subtracted from the sink at each simulation time step by using the thermostat method. The absolute values of the added and subtracted energies are usually equal, and their average is used to calculate the heat flux J through the system

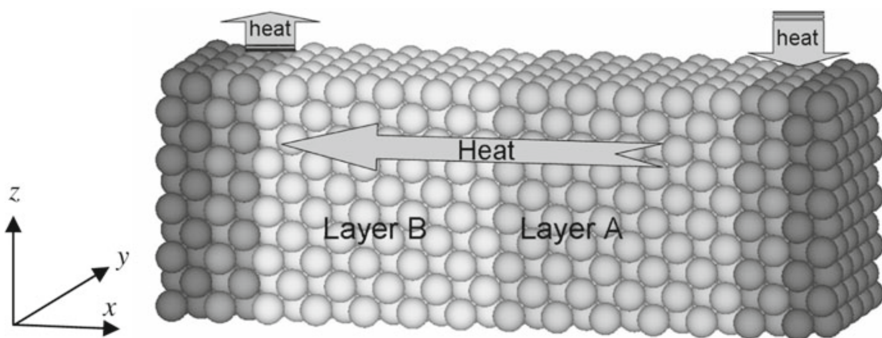

Fig. 1 Schematic picture of the bilayered nanofilm

along the x direction, $J = (\Delta\varepsilon_1 + \Delta\varepsilon_2) / (2S\Delta t)$, where S is the cross-sectional area and Δt is the simulation time step.

The atoms between the source and sink are referred to as "regular" atoms, and their length along the x direction is set as the composite film thickness L. The two layers have the same film thickness in the current work. The cross-plane thermal conductivity of the composite film is simply determined by Fourier's law as $\kappa = JL/(T_1 - T_2)$.

The periodic boundary condition is applied in the y and z directions. The velocity Verlet algorithm is used to numerically integrate the motion equations. The computing code was revised from Ref. [15]. The instantaneous temperature profile is determined classically from the average of the kinetic energy of the atoms in each atomic plane in the x direction. The simulation time step Δt is about 4.3 fs. A simulation usually takes a total of 1×10^6 steps, and the data of the last 5×10^5 time steps are used to calculate the thermal conductivity. In the simulation with the 5 UC × 5 UC section, the total time steps are expanded to 4×10^6 and the final data are from the last 3×10^6 steps to reduce the statistical fluctuation of the interface resistance.

3 Results and Discussion

The temperature profile for a bilayered material film, as an example, is shown in Fig. 2. The cross section of the simulation system is 10 UC × 10 UC, and its thickness is 20 UC. The temperature profiles for the simulations are reasonably linear for each individual film, and a clear temperature jump occurs at the interface between the layers, which indicates the presence of an interfacial thermal resistance. By a least-squares fit of the temperature in the two layers, the temperature difference of the two best-fit lines at the interface can be determined and is taken as the interfacial temperature difference. The interfacial thermal resistance is calculated using Eq. 1.

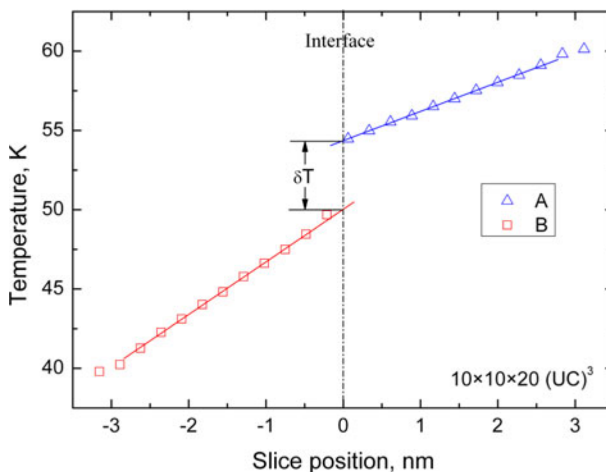

Fig. 2 Temperature profile of the bilayered film in which the atomic mass ratio of B/A is 5

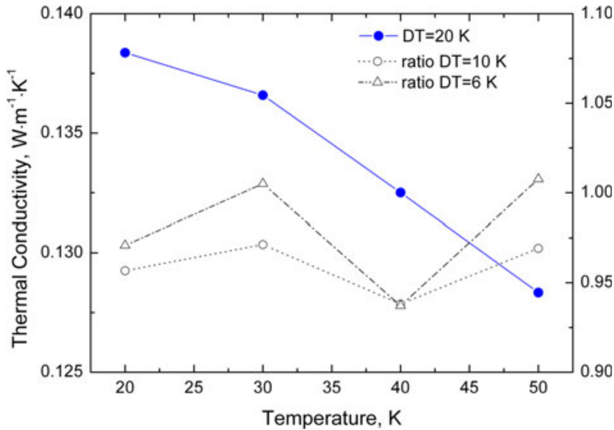

Fig. 3 Cross-plane thermal conductivity for different temperatures

Figure 3 shows the normal thermal conductivity plotted against temperature, where the system is 10 UC $\times$ 10 UC $\times$ 20 UC. The difference of the temperatures (DT) between the source and sink is set to be 20 K, and the average value is referred to as the system average temperature. As the average temperature increases from 20 K to 50 K, the thermal conductivity slowly and monotonically decreases. This decreasing trend is similar to that of solid argon [17], but it is slower than that reported. The reason is that the interfacial and boundary resistances contribute a major portion to the total resistance. The normalized thermal conductivities for DT = 10 K and 6 K cases with respect to that of DT = 20 K case are also plotted in Fig. 3, relative to the right-hand scale. The thermal conductivities change only within 6 % from that of the DT = 20 K case, which demonstrates that the DT value has no important influence on the thermal conductivity and the results with DT = 20 K are reasonable. In other words, the thermal conductivity is practically independent of the heat flux for DT < 20 K.

For the same system, the results of the temperature dependence of the interfacial thermal resistance are illustrated in Fig. 4. Similar to the thermal conductivity, the interfacial thermal resistance also decreases with increasing temperature. The reason is probably that, according to Ref. [18], the shared phonon density of states of the two materials at high temperature is higher than that at low temperature and thus the interface resistance is smaller at higher temperature. It is also found that the results are not much affected by the simulation DT values, and for the following cases, the DT values are all set to 20 K.

Changing the value of the mass ratio means changing the properties of the two materials, and that different interfaces can be obtained. For the system with a cross section of 10 UC $\times$ 10 UC and a length of 20 UC, the results in Fig. 5 obtained at 40 K display that the increment of interfacial thermal resistance varies almost linearly with the atomic mass ratio. Thus, the interfacial thermal resistance is greatly dependent on the materials on the two sides of the interface. With an increasing atomic mass ratio, the shared phonon density of states becomes smaller; thus, a higher interface resistance is produced.

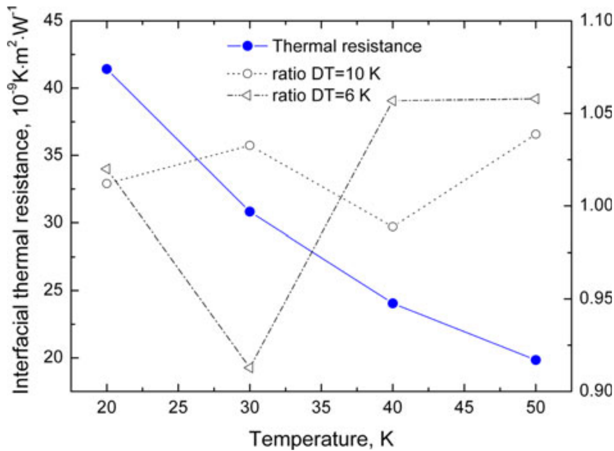

Fig. 4 Interfacial thermal resistance for different temperatures

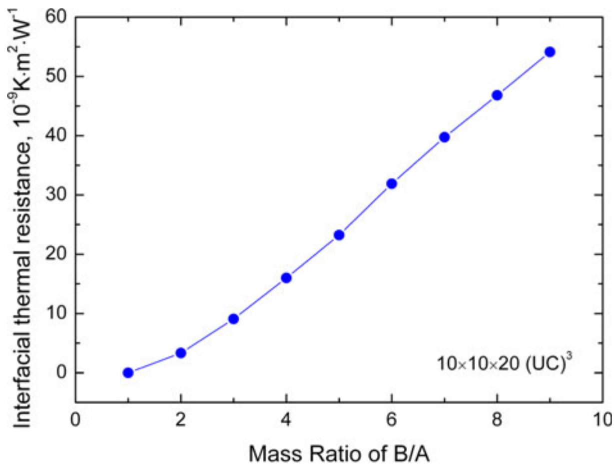

Fig. 5 Interfacial thermal resistance as a function of the atomic mass ratio of B/A

Due to the periodic boundary conditions in the in-plane directions, it is reasonable that the results for the thermal conductivity are independent of the cross-sectional area. The study of Lukes et al. [19] indicated that a cross section of 4 UC × 4 UC or larger could eliminate the boundary influence on the simulated thermal conductivity of a thin film, and a MD simulation of the Ar/Kr superlattice [13] also demonstrated that the thermal conductivity is independent of the cross section. Our simulations with different cross sections as shown in Fig. 6 also demonstrate that the cross section has no influence on the thermal conductivity of the composite film, except for the error bar of its fluctuation.

Although being independent of the heat flux, the thermal conductivity is heavily dependent on the film thickness at the nanoscale, which is due to the phonon scattering induced in the system by the heating and cooling regions. The data shown in Fig. 7

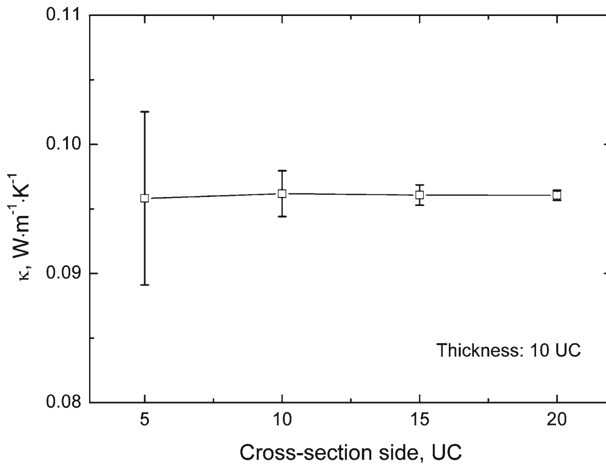

Fig. 6 Thermal conductivity as a function of the cross section

are obtained from the simulation with a cross section of 5 UC $\times$ 5 UC. The reduction of the cross section from 10 UC $\times$ 10 UC to 5 UC $\times$ 5 UC is due to computer limits, and it does not affect the final results according to the data in Fig. 6. As shown in Fig. 7a, the thermal conductivity increases smoothly with increasing film thickness, but the increment becomes smaller for a thicker film. It is because the limitation on the mean free path of phonons between the surface and interface gradually disappeared with a larger film thickness. Further analysis of the relationship between the thermal conductivity and thickness shows the linearity between L/κ and L, as shown in Fig. 7b. Actually, L/κ is equal to the total thermal resistance. The two lines in Fig. 7b are the least-squares fit curves of the data for 50 K and 20 K, and their intercepts represent the intrinsic thermal resistance, which includes the resistance at the interface and the boundary resistances near the heating and cooling zones. The intrinsic thermal resistance of 20 K is larger than that of 50 K. When the film thickness is large, the resistances of layer A and layer B are much larger than its intrinsic resistance, as shown in Fig. 7b, and thus the thermal conductivity for 20 K is larger than that for 50 K. When the thickness is small, the intrinsic resistance is a major contributor to the total resistance, and the thermal conductivity for 20 K is smaller due to the larger intrinsic resistance. That is why there is a crossing for a thickness of about 7 nm in Fig. 7a, b.

It is noted that the plot of L/κ vs. L is linear in Fig. 7b, which also means that $1/\kappa$ changes linearly with $1/L$. For a single film, with a decreasing phonon mean free path, a linear relationship should exist between the reciprocal of the thermal conductivity and that of the thickness [20,21]. Similarly, this reciprocal linear relationship still holds even though the system has two different layers. To understand the details of the thickness effect, the correlative temperature profiles are plotted in Fig. 8, where the slice position in the film is reduced according to its thickness, and the average temperature is 20 K. The temperature drop at the interface decreases with the film thickness, but the average interfacial temperature is almost constant.

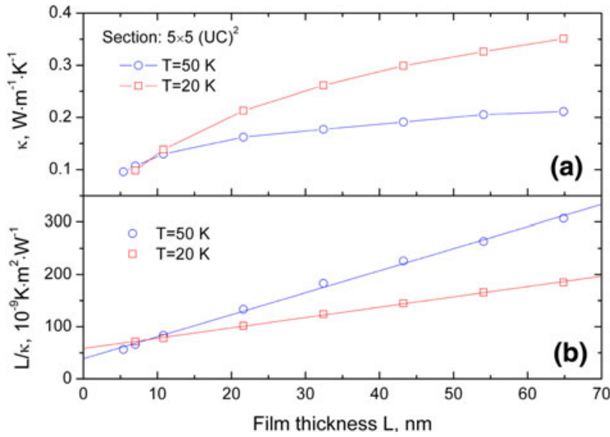

Fig. 7 Thermal conductivity as a function of the film thickness: (**a**) film thickness dependence of κ on L and (**b**) film thickness dependence of L/κ on L

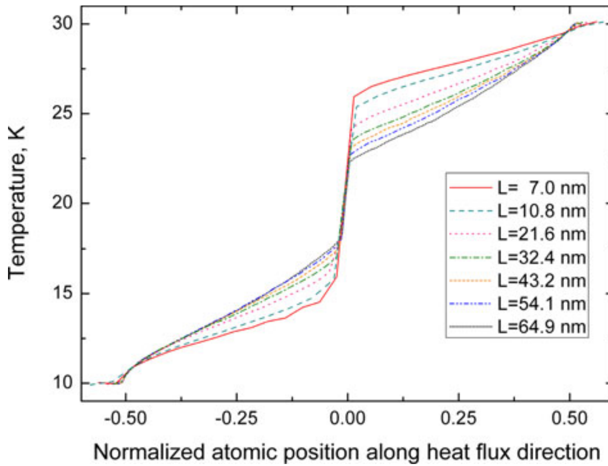

Fig. 8 Temperature profiles with different film thicknesses

The relationship of the interfacial thermal resistance and the film thickness is also investigated in addition to the thermal conductivity, as shown in Fig. 9. In a simulation with 1×10^6 steps, it is found that the temperature profile in the layers becomes flat and the interface temperature drop becomes very small for a large film thickness. A small fluctuation in the temperature profile leads to a very large change in the calculated interface resistance. To reduce the uncertainty, the run steps is expanded to 4×10^6, and the data from the last 3×10^6 time steps are used to obtain the final interfacial thermal resistance. For each film thickness, three trials are run and the averaged value is used as the interfacial resistance as shown in Fig. 9. The error bar in Fig. 9 is the fluctuation in the three runs with different initial velocity distributions. As indicated in Fig. 9, when the film thickness increases, the interfacial thermal resistance remains almost constant. This variation is different from the case of Ref. [13] in which there

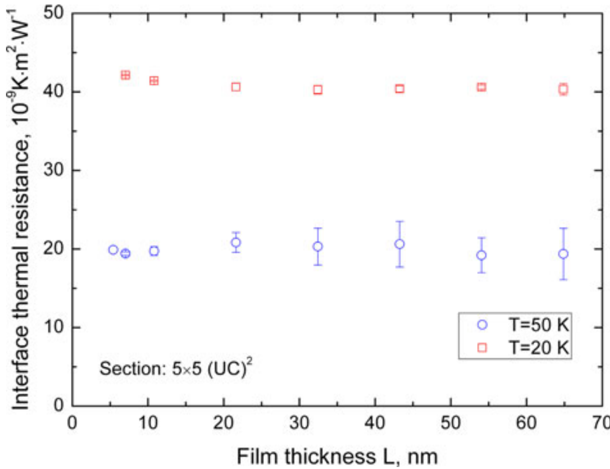

Fig. 9 Interfacial thermal resistance as a function of film thickness

exists an interface strain. In the present simulation the lattice constant is the same for both the layers, and there should be no strong strain in the film. The reason that the film thickness has no effect on the interfacial thermal resistance could be explained by the acoustic-mismatch model (AMM) [3], which gives the transmission coefficient t_{AB} for a phonon in layer A incident normal to the interface with layer B as

$$t_{AB} = \frac{4Z_A Z_B}{(Z_A + Z_B)^2} \tag{3}$$

where the acoustic impedance $Z = \rho c$, with ρ and c being the mass density and the speed of sound, respectively. When the film thickness varies, ρ and c do not change, which makes the acoustic impedance and the transmission coefficient constant. Thus, although the film thickness increases, the interfacial thermal resistance is still constant. The interfacial resistance at 20 K is larger than that at 50 K, which agrees with the results in Fig. 4.

On the other hand, according to Figs. 8 and 9, the increasing film thickness results in a decrease in the interfacial temperature drop, but the interface thermal resistance is constant. So the interfacial thermal resistance is also independent of the temperature drop at the interface or the heat current through the interface. It should be concluded that the interfacial thermal resistance is related with the properties of the two materials and an intrinsic property of a bilayered film.

4 Conclusions

The results of this work indicate that the interfacial thermal resistance plays an important role in heat conduction for bilayered nanofilms at the nanoscale. It is dependent on the temperature and film properties, and independent of the film thickness. It decreases with increasing temperature at the nanoscale. For a bilayered film with a thickness

from 5.4 nm to 64.9 nm, the reciprocal of its cross-plane thermal conductivity has a linear relationship with that of the film thickness.

Acknowledgment This work is supported by the National Natural Science Foundation of China (Contract No. 50776053).

References

1. P.L. Kapitza, J. Phys. (USSR) **4**, 181 (1941)
2. M. Khalatnikov, Zh. Eksp. Teor. Fiz. **22**, 687 (1952)
3. E.T. Swartz, R.O. Pohl, Rev. Mod. Phys. **61**, 605 (1989)
4. D.G. Cahill, W.K. Ford, K.E. Goodson, G.D. Mahan, G.A. Majumdar, H.J. Maris, R. Merlin, S.R. Phillpot, J. Appl. Phys. **93**, 793 (2003)
5. R.J. Stoner, H.J. Maris, Phys. Rev. B **48**, 16373 (1993)
6. R.M. Costescu, M.A. Wall, D.G. Cahill, Phys. Rev. B **67**, 054302 (2003)
7. H.K. Lyeo, D.G. Cahill, Phys. Rev. B **73**, 144301 (2006)
8. A. Maiti, G.D. Mahan, S.T. Pantelides, Solid State Commun. **102**, 517 (1997)
9. P.K. Schelling, S.R. Phillpot, P. Keblinski, J. Appl. Phys. **95**, 6082 (2004)
10. B.C. Daly, H.J. Maris, K. Imamura, S. Tamura, Phys. Rev. B **66**, 024301 (2002)
11. B.C. Daly, H.J. Maris, Y. Tanaka, S. Tamura, Phys. Rev. B **67**, 033308 (2003)
12. A.R. Abramson, C.L. Tien, A. Majumdar, J. Heat Transfer **124**, 963 (2002)
13. Y.F. Chen, D.Y. Li, J.K. Yang, Y.H. Wu, J.R. Lukes, A. Majumdar, Physica B **349**, 270 (2004)
14. X.G. Liang, L. Sun, Microscale Thermophys. Eng. **9**, 295 (2005)
15. D.C. Rapaport, *The Art of Molecular Dynamics Simulation*, 2nd edn. (University Press, Cambridge, 2004), pp. 11–43
16. P. Jund, R. Jullien, Phys. Rev. B **59**, 13707 (1999)
17. K.V. Tretiakov, S. Scandolo, J. Chem. Phys. **120**, 3765 (2004)
18. H.L. Zhong, J.R. Lukes, Phys. Rev. B **74**, 125403 (2006)
19. J.R. Lukes, D.Y. Li, X.G. Liang, C.L. Tien, J. Heat Transfer **122**, 536 (2000)
20. P.K. Schelling, S.R. Phillpot, P. Keblinski, Phys. Rev. B **65**, 144306 (2002)
21. P. Heino, Phys. Rev. B **71**, 144302 (2005)